Article ID: 1000-324X(2019)03-0335-06 **DOI:** 10.15541/jim20180273

Multi-doping in SnTe: Improvement of Thermoelectric Performance due to Lower Thermal Conductivity and Enhanced Power Factor

TAN Xiao-Fang[1,2], DUAN Si-Chen[1], WANG Hong-Xiang[1,3], WU Qing-Song[4], LI Miao-Miao[5], LIU Guo-Qiang[1,3], XU Jing-Tao[1,3], TAN Xiao-Jian[1,3], SHAO He-Zhu[1,3], JIANG Jun[1,3]

(1. Ningbo Institute of Materials Technology and Engineering, Chinese Academy of Sciences, Ningbo 315201, China; 2. Nano Science and Technology Institute, University of Science and Technology of China, Suzhou 215123, China; 3. University of Chinese Academy of Sciences, Beijing 100049, China; 4. Laboratory of Advanced Materials, Fudan University, Shanghai 200438, China; 5. College of Mechanics and Materials, Hohai University, Nanjing 210098, China)

Abstract: In recent years, tin telluride (SnTe) has attracted considerable interest due to its potential thermoelectric application as a lead-free rock-salt analogue of PbTe. However, pristine SnTe samples show high thermal conductivity and low Seebeck coefficients, resulting in poor thermoelectric performance. In this study, the thermoelectric performance of SnTe was enhanced by well-designed multi-doping, where significantly reduced thermal conductivity and improved Seebeck coefficients were achieved at the same time. The doped SnTe samples were prepared by hot pressing. The lattice thermal conductivity of SnTe samples is obviously decreased by alloying with Se and S. The transmission electron microscope shows the existence of larger amount of nano-precipitates and the lattice distortions in the alloyed samples. For example, the lattice thermal conductivity of $SnTe_{0.7}S_{0.15}Se_{0.15}$ sample is reduced to 0.99 $W\cdot m^{-1}\cdot K^{-1}$ at 300 K. The results reveal that the Seebeck coefficients are improved by introducing In resonant state in the band structure of SnTe. The experiments suggest the effectiveness of designed multi-doping in the thermoelectric performance enhancement of SnTe, and a promising *ZT* of 0.8 at 850 K is achieved in $Sn_{0.99}In_{0.01}Te_{0.7}S_{0.15}Se_{0.15}$. The discovery suggests that SnTe is a promising medium-temperature thermoelectric candidate.

Key words: tin telluride; thermoelectric performance; resonant state; lattice thermal conductivity

The conversion efficiency of thermoelectric material is quantified by the so-called *ZT* value defined as $\sigma S^2T/(\kappa_{lat} + \kappa_{ele})$, where σ, S, κ_{ele}, κ_{lat}, and T are the electrical conductivity, the Seebeck coefficient, electronic and lattice thermal conductivity, and absolute temperature, respectively[1-4]. The most commonly pursued approaches to enable high *ZT*s include the band structure manipulation for high power factor σS^2 by resonant levels near the Fermi level[5-11] or introducing band convergence[12-14], and phonon scattering enhancement by alloying or nanostructuring to minimize the thermal conductivity[15-29].

Over the last few years, SnTe has stepped into sight as a promising thermoelectric candidate due to its less toxic and a potential substitute of PbTe[21, 30]. But comparing to PbTe, SnTe suffers from a much lower *ZT* due to a smaller band gap (~0.18 eV) and the higher separation between the light-hole band at *L* and the heavy-hole band at ε (~ 0.3 eV)[31]. In addition, the relatively high thermal conductivity also limits its thermoelectric performance. Recent reports showed that the Seebeck coefficient of SnTe could be improved considerably by Cd, Mg, Mn, or Hg doping to converge the two valence bands and enlarge the band gap[32-43]. In doping in SnTe has also been found to create the resonant level inside the valence band and enhance the Seebeck coefficients around room temperature[21], which is similar to the Tl-doped PbTe system[5,11].

On the other hand, the remarkable decrease in the lattice thermal conductivity could also lead to obviously improved thermoelectric performance of SnTe *via* phonon scattering by solid solution point defects, secondary phase nanoprecipitates[27-28,44-45], and mesoscale grain boundaries[45-46]. For example, some nanoscale secondary phases such as CdS, HgTe, SrTe, Cu_2Se and Cu_2S, was introduced to regulate the thermal transport of SnTe, and

Received date: 2018-06-21; **Modified date:** 2018-09-06
Foundation item: National Key Research and Development Program of China (2016YFC0101801, 2017YFC0111602); Natural Science Foundation of Zhejiang Province (LY18A040008, LY18E020017); Zhejiang Provincial Science Fund for Distinguished Young Scholars (LR16E020001); Youth Innovation Promotion Association of CAS under Grant No. 2018337
Biography: TAN Xiao-Fang (1993–), female, Master. E-mail: txf082@mail.ustc.edu.cn
Corresponding author: XU Jing-Tao, professor. E-mail: xujingtao@nimte.ac.cn; TAN Xiao-Jian, associate professor. E-mail: tanxiaojian@nimte.ac.cn; JIANG Jun, professor. E-mail: jjun@nimte.ac.cn

the heat-carrying phonons were strongly scattered as expected[33-35,47-49]. Therefore, it is necessary to combine the Seebeck coefficient enhancement and designed phonon scattering to further improve the thermoelectric performance of SnTe materials.

In this work, we try to improve the thermoelectric performance of SnTe from the coexistence of resonant levels and secondary phases scattering. Firstly, the thermal conductivity of SnTe is decreased through secondary phases of SnS by S, Se doping. Then the optimized sample with 15mol% S and Se incorporated is used for the following In doping study. The thermoelectric properties are improved by multi-doping.

1 Experimental

Commercial elements Sn, Te, S, Se and In were used as starting materials. The materials with nominal compositions of $SnTe_{1-2x}S_xSe_x$ (x=0, 0.05, 0.1, and 0.15), and $Sn_{1-y}In_yTe_{0.7}S_{0.15}Se_{0.15}$ (y=0, 0.0025, 0.005, 0.01, and 0.015) were prepared by hot pressing[50-51]. X-ray diffraction (XRD) analysis was performed in a reflection geometry on a Bruker D8 diffractometer. The microstructures were investigated by the high resolution transmission electron microscope (JEOL 2100F), attached with an energy dispersive spectrometer (EDS). The samples were cut into bars with 10 mm×2 mm×2 mm for electrical property measurement and ϕ10 mm×2 mm for thermal transport property measurement. The Seebeck coefficient S and electrical conductivity σ were simultaneously measured using a ZEM-3 (ULVAC) instrument under a low-pressure helium atmosphere from room temperature to 850 K. The thermal conductivity was calculated from $\kappa=D\rho C_p$, where D is the thermal diffusivity, ρ is the density, and C_p is the specific heat. D was measured using the laser flash diffusivity method in a Netzsch LFA-457, ρ was measured by using Archimedes principle, and C_p was calculated from others data and our prebvious work[19,44,50]. The Hall coefficient R_H was measured at room temperature using a physical properties measurement system (Quantum Design, PPMS-9). The carrier concentration n and the hall mobility μ were estimated according to $n=1/(eR_H)$, and $\mu=\sigma R_H$ by using the single parabolic band approximation, respectively.

2 Results and Discussions

Figure 1 shows the total thermal conductivity κ_{tot} and lattice thermal conductivity of $SnTe_{1-2x}S_xSe_x$ (x=0, 0.05, 0.1, and 0.15) samples. The lattice thermal conductivity κ_{lat} is calculated by subtracting electrical thermal conductivity κ_{ele} from the total thermal conductivity, and the electrical thermal conductivity was calculated using the Wiedemann-Frenz relationship $\kappa_{ele}=L\sigma T$. It should be noted that the Lorenz number L is roughly obtained by fitting S using a single parabolic band model. The corresponding temperature dependent electrical conductivity σ and Seebeck coefficient S are summarized in Supporting Information.

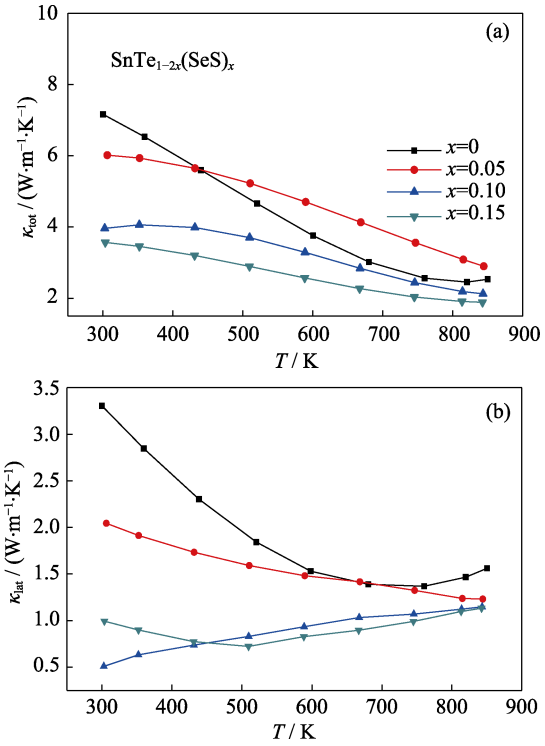

Fig. 1 Temperature-dependent (a) total thermal conductivities (κ_{tot}) and (b) lattice thermal conductivities (κ_{lat}) of $SnTe_{1-2x}S_xSe_x$ (x = 0, 0.05, 0.1, and 0.15) samples

As shown in Fig.1(b), the lattice thermal conductivities of $SnTe_{1-2x}S_xSe_x$ (x=0.05, 0.1, and 0.15) samples decrease significantly compared to that of pristine SnTe, which may be due to the excess phonon scattering by the solid solution and point defects. Considering that $SnTe_{1-2x}S_xSe_x$ with 15mol% S and Se exhibits the lowest κ_{lat}, x=0.15 is used for the following In doping investigation. Typically, the lattice thermal conductivity of $SnTe_{0.7}S_{0.15}Se_{0.15}$ sample is 0.99 $W\cdot m^{-1}\cdot K^{-1}$ at 300 K, mildly decreases to a minima of 0.72 $W\cdot m^{-1}\cdot K^{-1}$ at 509 K, and then slightly increases to 1.13 $W\cdot m^{-1}\cdot K^{-1}$ at 850 K.

Figure 2 presents the total and lattice thermal conductivity as a function of temperature of $Sn_{1-y}In_yTe_{0.7}S_{0.15}Se_{0.15}$ (y=0, 0.0025, 0.005, 0.01, and 0.015) samples. As shown, the total thermal conductivities all decrease with increasing temperature. With increasing In doping, the total thermal conductivity significantly decreases. For example, κ_{tot} decreases from 3.6 $W\cdot m^{-1}\cdot K^{-1}$ for y=0 to 2.1 $W\cdot m^{-1}\cdot K^{-1}$ for y=0.015 at room temperature, and decreases from 1.9 $W\cdot m^{-1}\cdot K^{-1}$ for y=0 to 1.7 $W\cdot m^{-1}\cdot K^{-1}$ for y=0.015 at 850 K.

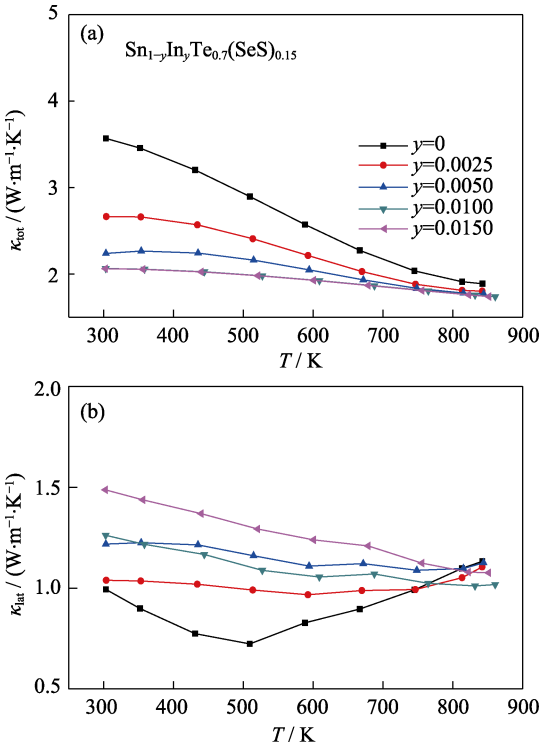

Fig. 2　Temperature-dependent (a) total thermal conductivities (κ_{tot}) and (b) lattice thermal conductivities (κ_{lat}) of $Sn_{1-y}In_yTe_{0.7}S_{0.15}Se_{0.15}$ (y=0, 0.0025, 0.005, 0.01, and 0.015) samples

As shown in Figure 2(b), the lattice thermal conductivity of In-doped $Sn_{1-y}In_yTe_{0.7}S_{0.15}Se_{0.15}$ increases from 0.99 Wm^{-1}·K^{-1} for y=0 to 1.48 W·m^{-1}·K^{-1} for y=0.0025 at room temperature, and decreases from 1.13 W·m^{-1}·K^{-1} for y=0 to 1.01 W·m^{-1}·K^{-1} for y=0.01 at 850 K. It is worth mentioning that the sample with y=0.0025 shows less temperature dependent, and κ_{lat} increases at elevated temperature, which is probably due to the bipolar diffusion. Typically, κ_{lat} of $Sn_{1-y}In_yTe_{0.7}S_{0.15}Se_{0.15}$ sample for y=0.0025 is 1.03 W·m^{-1}·K^{-1} at 300 K, slightly decreases to a minima of 0.96 W·m^{-1}·K^{-1} at 592 K, and then increases to 1.10 W·m^{-1}·K^{-1} at 850 K.

To gain deep understanding of suppressed lattice thermal conductivity in multi-doped SnTe, the microstructure of the samples was observed by using transmission electron microscope (TEM). Fig. 3(a) exhibits a medium-magnification of the multi-doped SnTe matrix along [004] orientation. Small precipitates (red circles in Fig. 3(b)) are observed in the matrix , and only one set of Bragg diffraction spots is observed in the inset selected area diffraction (SAD) pattern of the corresponding area (bottom-right in Fig. 3(a)). The composition contrast can be evidenced by the energy-dispersive X-ray spectroscopy (EDS) (Fig. 3(b)) obtained from the precipitates that exhibit characteristic peaks for In, S and Se.

High-resolution TEM (HRTEM) image in Fig. 3(c) shows the matrix SnTe (200) and the secondary phase SnS

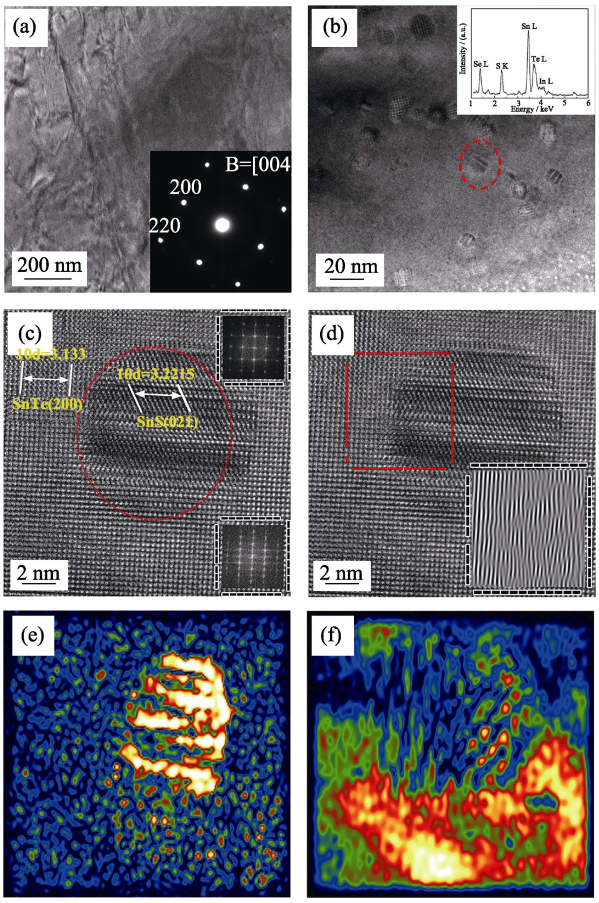

Fig. 3　Microstructures of $Sn_{0.99}In_{0.01}Te_{0.7}S_{0.15}Se_{0.15}$
(a) Medium-magnification TEM and (b) low-magnification images show the presence of nanoscale secondary phase; The inset in (a) is the SAED pattern along [004]; (c) HRTEM image focusing on the secondary phase with distorted connection between the precipitate and the matrix; The top-right and bottom-right insets are the respective FFT images showing lattice distortion between them; (d) the same TEM image with (c) showing the IFFT image (the bottom-right inset) of the selected region reflecting lattice distortion; and strain maps reflect high strain states inside (e) and around (f) the precipitates

(021). Accordingly, the respective fast Fourier transformation (FFT) image (the top-right and bottom-right inset in Fig. 3(c)) shows no obvious peak splitting and reflects an endotaxial relationship between the matrix and secondary phase. In Fig. 3(d), the lattice distortion is more obvious to be seen in the inverse fast Fourier transformation (IFFT) image (the bottom-right inset).

To further analyze the possible strain around the precipitates and the connection between the lattice distortions, high-quality HRTEM images in Figure 3(e-f) were carried out by geometric phase analysis, which is a semi-quantitative lattice image-processing approach for revealing spatial distribution of relative elastic strain. As shown, the strains exist in the secondary phases and extensively concentrate around them. The strains mainly result from the lattice or orientation mismatch between the matrix and the secondary phase, and it is a pervasive defect effect associated with point defects and disloca-

tion. These high density of strains around the secondary phase plays a significant role on increasing the phonon scattering. In addition, the atomic-scale point defects and dislocation could scatter short-wavelength phonon efficiently. These multiscale phonon scattering mechanisms contribute to the low lattice thermal conductivity.

The temperature dependence of electrical conductivity for $Sn_{1-y}In_yTe_{0.7}S_{0.15}Se_{0.15}$ (y=0, 0.0025, 0.005, 0.01, and 0.015) samples are shown in Fig. 4(a). It may be seen that the electrical conductivity decreases with increasing temperature from 300 K to 850 K, showing a degenerate semiconductor behavior. At a particular temperature, the electrical conductivity monotonously decreases with increasing In content. For example, the electrical conductivity at room temperature significantly decreases from ~ 3480 S·cm^{-1} for y=0 to~910 S·cm^{-1} for y=0.015, which can be attributed to the reduced carrier mobility of sample as summarized in Table 1.

In Fig. 4(b), the temperature dependent Seebeck coefficients of $Sn_{1-y}In_yTe_{0.7}S_{0.15}Se_{0.15}$ (y=0, 0.0025, 0.005, 0.01, and 0.015) samples are presented. It should be noted that the Seebeck coefficients of In doped samples are enhanced with respect to the $SnTe_{0.7}S_{0.15}Se_{0.15}$ over the entire temperature range. Especially, the Seebeck coefficient at room temperature increases from 7.6 μV·K^{-1} for y=0 to 71 μV·K^{-1} for y=0.015, and the improvement is almost an order of magnitude. With increasing temperature, the enhancement slows down, the Seebeck coefficient of $SnTe_{0.7}S_{0.15}Se_{0.15}In_{0.015}$ at 850 K is 180 μV·K^{-1} and slightly higher than 151 μV·K^{-1} of $SnTe_{0.7}S_{0.15}Se_{0.15}$. Such a subdued enhancement of Seebeck coefficient at higher temperature is mainly due to the downshift of the Fermi level, where the introduced resonant state no longer works[34,51-52].

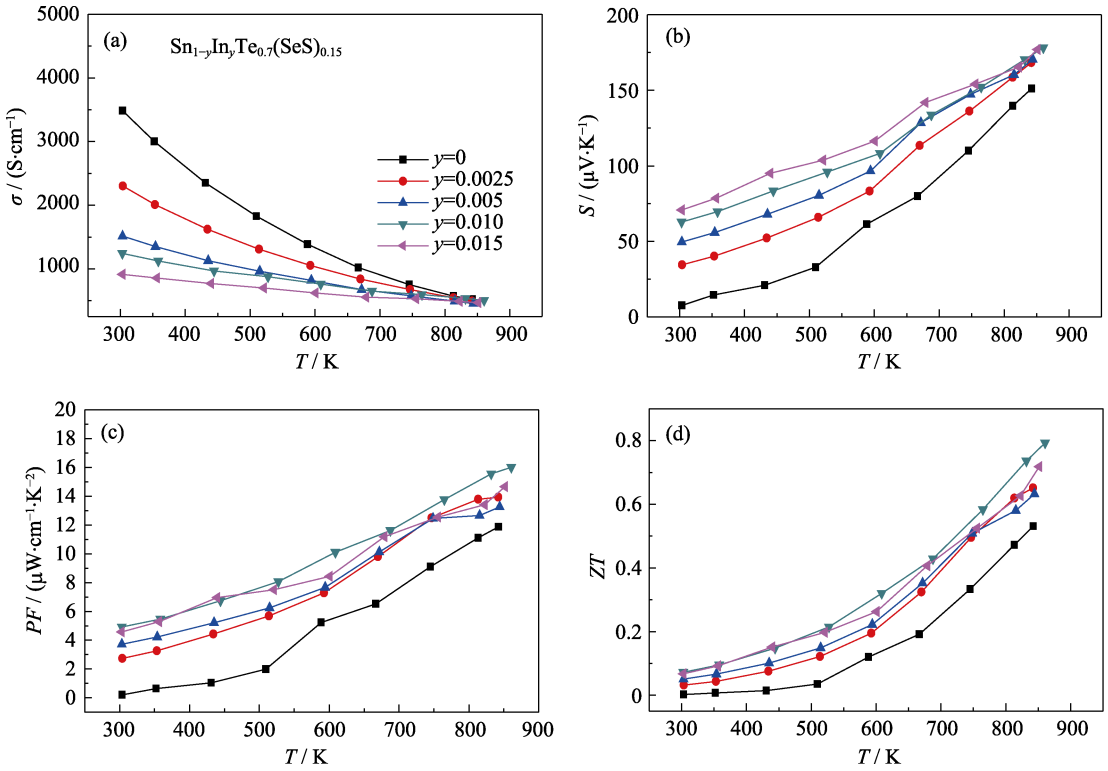

Fig. 4 Temperature dependent thermoelectric properties: (a) electrical conductivity σ, (b) the Seebeck coefficients S, (c) the power factors $S^2\sigma$, and (d) ZT values for $Sn_{1-y}In_yTe_{0.7}S_{0.15}Se_{0.15}$ (y=0, 0.0025, 0.005, 0.01, and 0.015) samples

Table 1 The density ρ, hole concentration n, mobility μ, electrical conductivity σ, Seebeck coefficient S, and power factor $S^2\sigma$ for $Sn_{1-y}In_yTe_{0.7}S_{0.15}Se_{0.15}$ (y=0, 0.0025, 0.005, 0.01, and 0.015) samples at room temperature

Samples	ρ/(g·cm^{-3})	N/(× 10^{20}, cm^{-3})	μ/(cm^2·V^{-1}·s^{-1})	σ/(S·cm^{-1})	S/(μV·K^{-1})	$S^2\sigma$/(μW·cm^{-1}·K^{-2})
y=0	6.247	1.3	164	3480	7.6	0.2
y=0.0025	6.209	1.4	100	2300	34	2.7
y=0.005	6.161	1.6	57	1510	50	3.7
y=0.01	6.161	2.0	39	1240	63	4.9
y=0.015	6.195	2.2	26	910	71	4.6

The power factor as a function of temperature for $Sn_{1-y}In_yTe_{0.7}S_{0.15}Se_{0.15}$ (y=0, 0.0025, 0.005, 0.01, and 0.015) samples is shown in Fig. 4(c). Because of the increased Seebeck coefficients, the power factors of In-doped samples are obviously enhanced as compared with that of $SnTe_{0.7}S_{0.15}Se_{0.15}$. If we focus on $SnTe_{0.7}S_{0.15}Se_{0.15}In_{0.01}$, the power factor is seen to rise almost linearly from 4.9 $\mu W\cdot cm^{-1}\cdot K^{-2}$ at room temperature to 16 $\mu W\cdot cm^{-1}\cdot K^{-2}$ at 850 K. Such enhancement of power factor is achieved mainly resulted from the resonant level effect in In-doped $SnTe_{0.7}S_{0.15}Se_{0.15}$. In Fig. 4(d), the *ZT* values are presented as a function of temperature for all In-doped $SnTe_{0.7}S_{0.15}Se_{0.15}$ samples. The highest *ZT* value reaches 0.8 at 850 K for 1mol% In-doped $SnTe_{0.7}S_{0.15}Se_{0.15}$, which shows the largest power factor and the lowest lattice thermal conductivity.

3 Conclusions

This work demonstrats that the *ZT* value of SnTe can reach 0.8 at 850 K by well-designed multi-doping. The improved thermoelectric performance of $Sn_{0.99}In_{0.01}Te_{0.7}S_{0.15}Se_{0.15}$ is accomplished by combination of reduced lattice thermal conductivity and enhanced power factor. The former mainly results from the secondary phase scattering by alloying Se, S, while the later mainly results from the resonant state by In doping. This work suggests that SnTe-based materials are important candidates for thermoelectric power generation and the well-designed multi-doping in SnTe is a promising approach to optimize the thermoelectric properties.

References

[1] SOOTSMAN J R, CHUNG D Y, KANATZIDIS M G. New and old concepts in thermoelectric materials. *Angewandte Chemie International Edition*, 2009, **48(46):** 8616–8639.

[2] KANATZIDIS M G. Nanostructured thermoelectrics: the new paradigm? *Chemistry of Materials*, 2009, **22(3):** 648–659.

[3] ZHAO L D, DRAVID V P, KANATZIDIS M G. The panoscopic approach to high performance thermoelectrics. *Energy & Environmental Science*, 2014, **7(1):** 251–268.

[4] VINEIS C J, SHAKOURI A, MAJUMDAR A, *et al*. Nanostructured thermoelectrics: big efficiency gains from small features. *Advanced Materials*, 2010, **22(36):** 3970–3980.

[5] HEREMANS J P, JOVOVIC V, TOBERER E S, *et al*. Enhancement of thermoelectric efficiency in PbTe by distortion of the electronic density of states. *Science*, 2008, **321(5888):** 554–557.

[6] JAWORSKI C M, KULBACHINSKII V, HEREMANS J P. Resonant level formed by tin in Bi_2Te_3 and the enhancement of room-temperature thermoelectric power. *Physical Review B*, 2009, **80(23):** 233201–1–4.

[7] BILC D, MAHANTI S D, QUAREZ E, *et al*. Resonant states in the electronic structure of the high performance thermoelectrics $AgPb_mSbTe_{2+m}$: the role of Ag-Sb microstructures. *Physical Review Letters*, 2004, **93(14):** 146403–1–4.

[8] AHN K, HAN M K, HE J, *et al*. Exploring resonance levels and nanostructuring in the PbTe-CdTe system and enhancement of the thermoelectric figure of merit. *Journal of the American Chemical Society*, 2010, **132(14):** 5227–5235.

[9] AHMAD S, MAHANTI S D, HOANG K, *et al*. *Ab initio* studies of the electronic structure of defects in PbTe. *Physical Review B*, 2006, **74(15):** 155205–1–13.

[10] ZHANG Q, WANG H, LIU W, *et al*. Enhancement of thermoelectric figure-of-merit by resonant states of aluminium doping in lead selenide. *Energy & Environmental Science*, 2012, **5(1):** 5246–5251.

[11] HEREMANS J P, WIENDLOCHA B, CHAMOIRE A M. Resonant levels in bulk thermoelectric semiconductors. *Energy & Environmental Science*, 2012, **5(2):** 5510–5530.

[12] PEI Y, SHI X, LALONDE A, *et al*. Convergence of electronic bands for high performance bulk thermoelectrics. *Nature*, 2011, **473(7345):** 66.

[13] LIU W, TAN X, YIN K, *et al*. Convergence of conduction bands as a means of enhancing thermoelectric performance of n-type $Mg_2Si_{1-x}Sn_x$ solid solutions. *Physical Review Letters*, 2012, **108(16):** 166601–1–5.

[14] ZHAO L D, WU H J, HAO S Q, *et al*. All-scale hierarchical thermoelectrics: MgTe in PbTe facilitates valence band convergence and suppresses bipolar thermal transport for high performance. *Energy & Environmental Science*, 2013, **6(11):** 3346–3355.

[15] YANG J, MEISNER G P, CHEN L. Strain field fluctuation effects on lattice thermal conductivity of ZrNiSn-based thermoelectric compounds. *Applied Physics Letters*, 2004, **85(7):** 1140–1142.

[16] ABELES B. Lattice thermal conductivity of disordered semiconductor alloys at high temperatures. *Physical Review*, 1963, **131(5):** 1906–1911.

[17] ZEIER W G, PEI Y, POMREHM G, *et al*. Phonon scattering through a local anisotropic structural disorder in the thermoelectric solid solution $Cu_2Zn_{1-x}Fe_xGeSe_4$. *Journal of the American Chemical Society*, 2013, **135(2):** 726–732.

[18] TAN G, LIU W, CHI H, *et al*. Realization of high thermoelectric performance in p-type unfilled ternary skutterudites $FeSb_{2+x}Te_{1-x}$ *via* band structure modification and significant point defect scattering. *Acta Materialia*, 2013, **61(20):** 7693–7704.

[19] ZHAO L D, TAN G, HAO S, *et al*. Ultrahigh power factor and thermoelectric performance in hole-doped single-crystal SnSe. *Science*, 2015, **351(6269):** 141–144.

[20] MINNICH A J, DRESSELHAUS M S, REN Z F, *et al*. Bulk nanostructured thermoelectric materials: current research and future prospects. *Energy & Environmental Science*, 2009, **2(5):** 466– 479.

[21] ZHANG Q, LIAO B, LAN Y, *et al*. High thermoelectric performance by resonant dopant indium in nanostructured SnTe. *Proceedings of the National Academy of Sciences*, 2013, **110(33):** 13261–13266.

[22] TAN G, LIU W, WANG S, *et al*. Rapid preparation of $CeFe_4Sb_{12}$ Skutterudite by melt spinning: rich nanostructures and high thermoelectric performance. *Journal of Materials Chemistry A*, 2013, **1(40):** 12657–12668.

[23] ZHAO L D, LO S H, HE J, *et al*. High performance thermoelectrics from earth-abundant materials: enhanced figure of merit in PbS by second phase nanostructures. *Journal of the American Chemical Society*, 2011, **133(50):** 20476–20487.

[24] ZHAO L D, HE J, WU C I, *et al*. Thermoelectrics with earth abundant elements: high performance p-type PbS nanostructured with SrS and CaS. *Journal of the American Chemical Society*, 2012, **134(18):** 7902–7912.

[25] ZHAO L D, HE J, HAO S, *et al*. Raising the thermoelectric performance of p-type PbS with endotaxial nanostructuring and valence-band offset engineering using CdS and ZnS. *Journal of the American Chemical Society*, 2012, **134(39):** 16327–16336.

[26] LEE Y, LO S H, ANDROULAKIS J, *et al*. High-performance tellurium-free thermoelectrics: all-scale hierarchical structuring of p-type PbSe-MSe systems (M=Ca, Sr, Ba). *Journal of the American Chemical Society*, 2013, **135(13):** 5152–5160.

[27] BISWAS K, HE J, ZHANG Q, *et al*. Strained endotaxial nanostructures with high thermoelectric figure of merit. *Nature Chemistry*, 2011, **3(2):** 160–166.

[28] BISWAS K, HE J, BLUM I D, *et al*. High-performance bulk thermoelectrics with all-scale hierarchical architectures. *Nature*, 2012, **489(7416):** 414–418.

[29] TAN G, ZHENG Y, TANG X. High thermoelectric performance of nonequilibrium synthesized $CeFe_4Sb_{12}$ composite with multi-scaled nanostructures. *Applied Physics Letters*, 2013, **103(18):** 7837–1–5.
[30] TAN G J, SHI F Y, HAO S Q, *et al*. Valence band modification and high thermoelectric performance in SnTe heavily alloyed with MnTe. *Journal of the American Chemical Society*, 2015, **137(35):** 11507–11516.
[31] ROGERS L M. Drift mobility of light-mass holes in PbTe heavily doped with Na. *Journal of Physics D Applied Physics*, 1968, **1(8):** 1067.
[32] HE J, XU J, LIU G, *et al*. Enhanced thermopower in rock-salt SnTe-CdTe from band convergence. *RSC Advances*, 2016, **6(38):** 32189–32192.
[33] TAN G, ZHAO L D, SHI F, *et al*. High thermoelectric performance of p-type SnTe *via* a synergistic band engineering and nanostructuring approach. *Journal of the American Chemical Society*, 2014, **136(19):** 7006–7017.
[34] TAN G J, SHI F Y, HAO S Q, *et al*. Codoping in SnTe: enhancement of thermoelectric performance through synergy of resonance levels and band convergence. *Journal of the American Chemical Society*, 2015, **137(15):** 5100–5112.
[35] TAN G, SHI F, DOAK J, *et al*. Extraordinary role of Hg in enhancing the thermoelectric performance of p-type SnTe. *Energy & Environmental Science*, 2014, **8(1):** 267–277.
[36] WEN L, ZHENG L, GE B, *et al*. Promoting SnTe as an eco-friendly solution for p-PbTe thermoelectric *via* band convergence and interstitial defects. *Advanced Materials*, 2017, **29(17):** 1605887–1–8.
[37] HE J, TAN X, XU J, *et al*. Valence band engineering and thermoelectric performance optimization in SnTe by Mn-alloying *via* a zone-melting method. *Journal of Materials Chemistry A*, 2015, **3(39):** 19974–19979.
[38] TAN G J, SHI F Y, HAO S Q, *et al*. Valence band modification and high thermoelectric performance in SnTe heavily alloyed with MnTe. *Journal of the American Chemical Society*, 2015, **137(35):** 11507–11516.
[39] LI W, CHEN Z, LIN S, *et al*. Band and scattering tuning for high performance thermoelectric $Sn_{1-x}Mn_xTe$ alloys. *Journal of Materiomics*, 2015, **1(4):** 307–315.
[40] ZHENG L, LI W, LIN S, *et al*. Interstitial defects improving thermoelectric SnTe in addition to band convergence. *ACS Energy Letters*, 2017, **2(3):** 563–568.
[41] WU H, CHANG C, FENG D, *et al*. Synergistically optimized electrical and thermal transport properties of SnTe *via* alloying high-solubility MnTe. *Energy & Environmental Science*, 2015, **8(11):** 3298–3312.
[42] BANIK A, SHENOY U S, ANAND S, *et al*. Mg alloying in SnTe facilitates valence band convergence and optimizes thermoelectric properties. *Chemistry of Materials*, 2015, **27(2):** 581–587.
[43] TAN X, SHAO H, HU T, *et al*. High thermoelectric performance in two-dimensional graphyne sheets predicted by first-principles calculations. *Physical Chemistry Chemical Physics*, 2015, **17(35):** 22872–22881.
[44] WU H, LU X, WANG G, *et al*. Sodium-doped tin sulfide single crystal: a nontoxic earth-abundant material with high thermoelectric performance. *Advanced Energy Materials*, 2018, **8(20):** 1800087–1–8.
[45] ZHAO L D, HAO S, LO S H, *et al*. High thermoelectric performance *via* hierarchical compositionally alloyed nanostructures. *Journal of the American Chemical Society*, 2013, **135(19):** 7364–7370.
[46] POUDEL B, HAO Q, MA Y, *et al*. High thermoelectric performance of nanostructured bismuth antimony telluride bulk alloys. *Science*, 2008, **320(5876):** 634–638.
[47] ZHAO L D, ZHANG X, WU H, *et al*. Enhanced thermoelectric properties in the counter-doped SnTe system with strained endotaxial SrTe. *Journal of the American Chemical Society*, 2016, **138(7):** 2366–2373.
[48] LIU H, SHI X, XU F, *et al*. Copper ion liquid-like thermoelectrics. *Nature Materials*, 2012, **11(5):** 422–425.
[49] HEY, DAY T, ZHANG T, *et al*. High thermoelectric performance in non-toxic earth-abundant copper sulfide. *Advanced Materials*, 2014, **26(23):** 3974–3978.
[50] ANANYA B, KANISHKA B. Lead-free thermoelectrics: promising thermoelectric performance in p-type $SnTe_{1-x}Se_x$ system. *Journal of Materials Chemistry A*, 2014, **2(25):** 9620–9625.
[51] TAN X, TAN X, LIU G, *et al*. Optimizing the thermoelectric performance of In-Cd codoped SnTe by introducing Sn vacancies. *Journal of Materials Chemistry C*, 2017, **5(30):** 7504–7509.
[52] TAN X J, LIU G Q, XU J T, *et al*. Element-selective resonant state in M-doped SnTe (M=Ga, In, and Tl). *Physical Chemistry Chemical Physics*, 2016, **18(30):** 20635–20639.

多掺杂协同调控碲化锡热导率和功率因子提升热电性能

檀小芳[1,2], 端思晨[1], 王泓翔[1,3], 吴庆松[4], 李苗苗[5], 刘国强[1,3],
徐静涛[1,3], 谈小建[1,3], 邵和助[1,3], 蒋 俊[1,3]

(1. 中国科学院 宁波材料技术与工程研究所, 宁波 315201; 2. 中国科学技术大学 纳米科学技术学院, 苏州 215123; 3. 中国科学院大学, 北京 100049; 4. 复旦大学 先进材料实验室, 上海 200438; 5. 河海大学 力学与材料学院, 南京 210098)

摘 要: 碲化锡(SnTe)是一种碲化铅的无铅替代物, 在热电领域有广阔的应用前景。但是, 纯相碲化锡样品具有较高的热导率与较低的塞贝克系数, 导致热电性能较差。本研究通过多重掺杂可以显著降低热导率, 提升塞贝克系数, 从而提升热电性能。SnTe 热压样品的晶格热导率随着 Se 和 S 的引入明显降低, 比如 $SnTe_{0.7}S_{0.15}Se_{0.15}$ 室温下晶格热导率仅为 0.99 $W\cdot m^{-1}\cdot K^{-1}$。透射电子显微镜显示, SnTe 掺杂样品内存在大量的纳米沉淀相与晶格位错。在此基础上, 掺杂 In 在价带顶引入共振态大幅提高了样品的塞贝克系数。实验表明通过多重掺杂可以有效提升碲化锡的热电性能, 其中样品 $Sn_{0.99}In_{0.01}Te_{0.7}S_{0.15}Se_{0.15}$ 在 850 K 时峰值 *ZT* 值达到 0.8, 这说明碲化锡的确是一种有应用前景的中温区热电材料。

关 键 词: 碲化锡; 热电性能; 共振态; 晶格热导率

中图分类号: TQ174 **文献标识码:** A

Supporting Information:

Multi-doping in SnTe: Improvement of Thermoelectric Performance due to Lower Thermal Conductivity and Enhanced Power Factor

TAN Xiao-Fang[1,2], DUAN Si-Chen[1], WANG Hong-Xiang[1,3], WU Qing-Song[4], LI Miao-Miao[5], LIU Guo-Qiang[1,3], XU Jing-Tao[1,3], TAN Xiao-Jian[1,3], SHAO He-Zhu[1,3], JIANG Jun[1,3]

(1. Ningbo Institute of Materials Technology and Engineering, Chinese Academy of Science, Ningbo 315201, China; 2. Nano Science and Technology Institute, University of Science and Technology of China, Suzhou 215123, China; 3. University of Chinese Academy of Sciences, Beijing 100049, China; 4. Laboratory of Advanced Materials, Fudan University, Shanghai 200438, China; 5. College of Mechanics and Materials, Hohai University, Nanjing 210098, China)

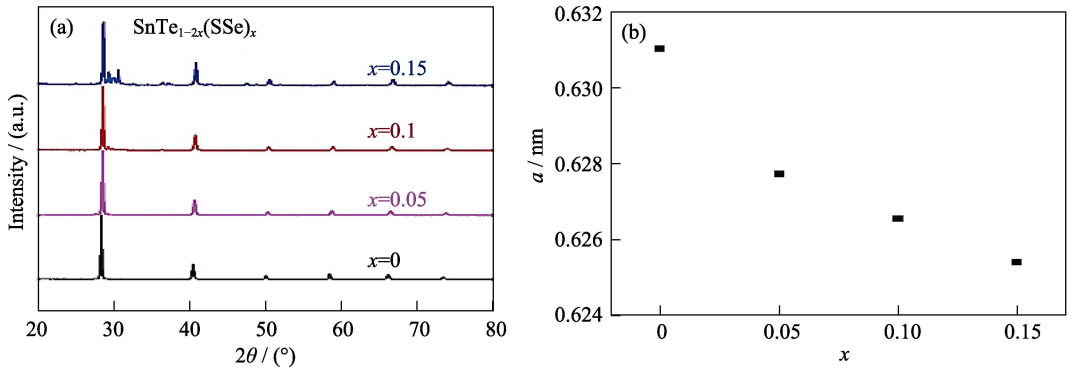

Fig. S1　Room temperature (a) powder XRD patterns, (b) lattice parameter of $SnTe_{1-2x}S_xSe_x$ (x=0, 0.05, 0.1, and 0.15) samples

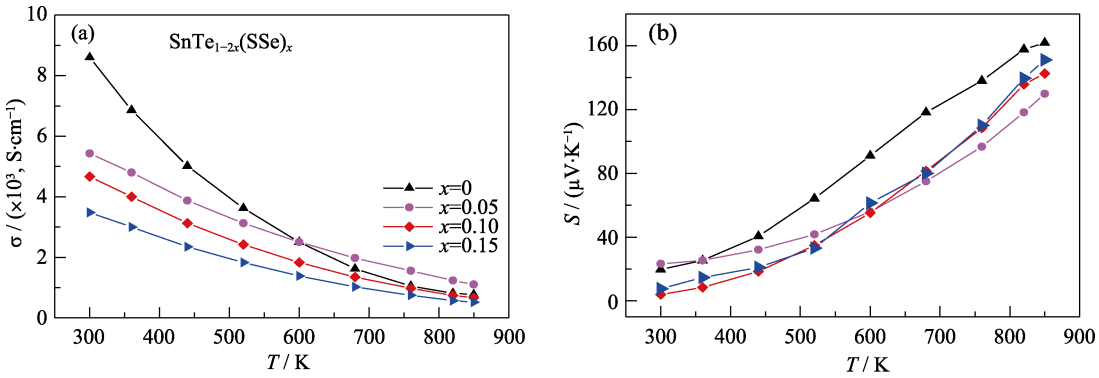

Fig. S2　Temperature dependent (a) electrical conductivity and (b) Seebeck coefficient of $SnTe_{1-2x}S_xSe_x$ (x=0, 0.05, 0.1, and 0.15) samples

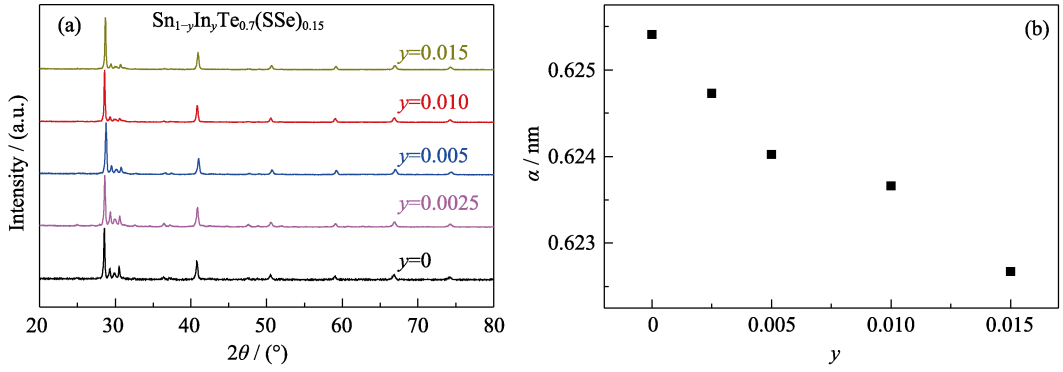

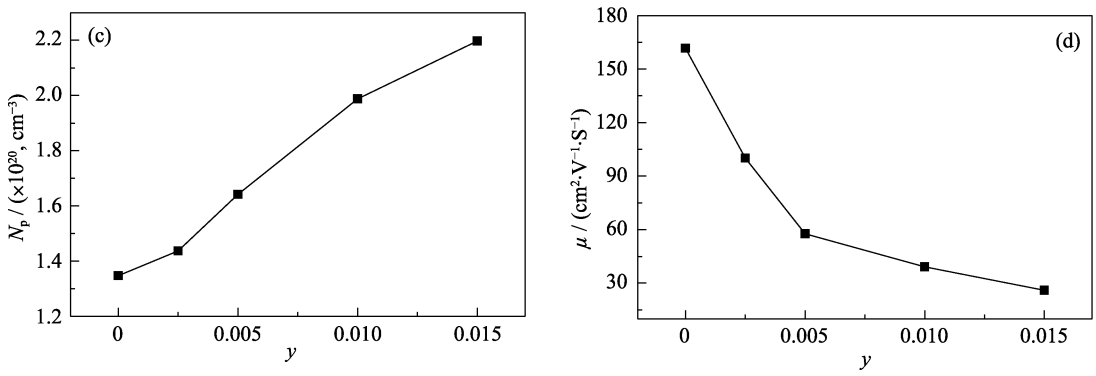

Fig. S3 Room temperature (a) powder XRD patterns, (b) lattice parameter a, (c) Hall carrier density N_p, and (d) carrier mobility μ of $Sn_{1-y}In_yTe_{0.7}S_{0.15}Se_{0.15}$ (y=0, 0.0025, 0.005, 0.01, and 0.015) samples

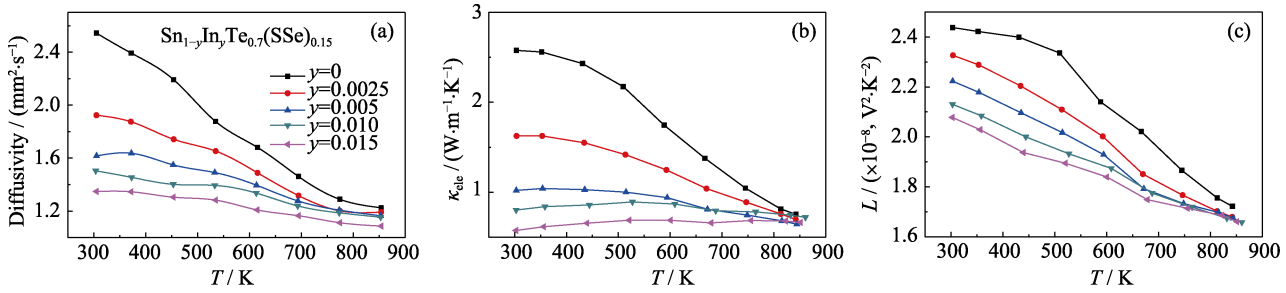

Fig. S4 Temperature dependent heat diffusivity of $Sn_{1-y}In_yTe_{0.7}S_{0.15}Se_{0.15}$ (y=0, 0.0025, 0.005, 0.01, and 0.015) samples

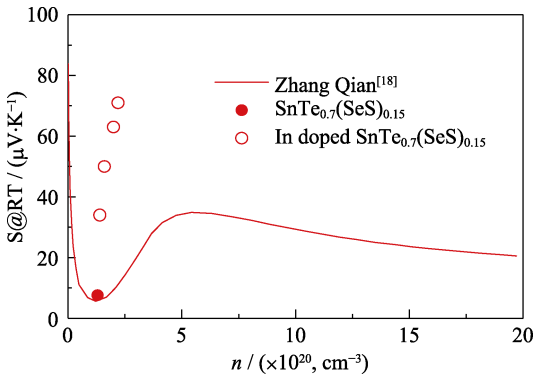

Fig. S5 Room temperature Pisarenko plot for $Sn_{1-y}In_yTe_{0.7}(SeS)_{0.15}$ (y=0, 0.0025, 0.005, 0.01, 0.015). The solid curve is experted from Zhang[18]